Sea ice interannual variability and sensitivity to fall oceanic conditions and winter air temperature in the Gulf of St. Lawrence, Canada.

Peter S. Galbraith[1], Caroline Sévigny[2], Daniel Bourgault[3], and Dany Dumont[3]

[1]Fisheries and Oceans Canada, Québec Region, Maurice Lamontagne Institute, P.O. Box 1000, Mont-Joli, Qc, Canada, G5H 3Z4
[2]Environment and Climate Change Canada, 801-1550 avenue D'Estimauville Québec, Qc, G1J 0C3
[3]Institut de sciences de la mer de Rimouski, Université du Québec à Rimouski, 310 allée des Ursulines, Rimouski, Qc, Canada G5L 3A1

Key Points:

- Seasonal maximum sea ice area and first occurrence are predictable with at most 36 to 44 days of lead time in the Gulf of St Lawrence
- Seasonal sea ice severity metrics (duration, maximum area and estimated volume) are shown to be related to winter air temperatures
- The only six nearly ice-free winters correspond to the warmest winter air temperatures over the Gulf

Corresponding author: Peter S. Galbraith, Peter.Galbraith@dfo-mpo.gc.ca

Abstract

The Gulf of St. Lawrence has been nearly free of sea ice in the winter six times in its recorded history, four of which have occurred since 2010. This study examines the inter-annual variability of sea ice cover characteristics (1969-2024) and winter mixed layer heat content (1996-2024), their sensitivity to fall oceanic conditions (since fall of 1995) and to winter air temperatures. The study finds no relationship between fall oceanic conditions with either the first occurrence of sea ice, maximum seasonal estimated volume or winter mixed layer heat content. However, it shows that the first occurrence of sea ice in the northwestern Gulf is related to the timing of sea surface temperature crossing the 1°C threshold with a lag time of 30 to 37 days, and with air temperature dropping below -2°C with a lag of 37 to 44 days; longer lags have weak correlations. The seasonal maximum conditions in area or estimated volume can be estimated by the preceding measurements of the same metrics with a lead time of only 29 days for volume and 36 days for area. The average air temperature over the Gulf between December and February or March is highly correlated to seasonal maximum sea ice area and estimated volume, as well as ice season duration. The six nearly ice-free winters correspond to the warmest December to February (or December to March) average air temperatures over the Gulf. A warming of $>$ 1.9°C–2.4°C (DJFM) or $>$ 2.2°C–2.9°C (DJF) above the 1991-2020 climatology leads to nearly ice-free conditions.

Plain Language Summary

The first occurrence and seasonal severity of sea ice in the Gulf of St Lawrence are shown to not be related to early fall ocean conditions. Atmospheric conditions prevalent when water temperature approaches the freezing point are drivers of first occurrence and can be used to predict onset of sea ice in the northwest Gulf with about 37 to 44 days of lead time. Seasonal sea ice severity metrics (duration, maximum area and estimated volume) are shown to be related to winter air temperatures. The seasonal maximum conditions in area or estimated volume can be estimated by the preceding measurements of the same metrics with a lead time of only 29 days for volume and 36 days for area. Six nearly ice-free winters correspond to the warmest December to February (or December to March) average air temperatures over the Gulf, providing the thresholds required for future climate warming to result in a nearly ice-free Gulf of St. Lawrence.

1 Introduction

The Gulf of St. Lawrence (GSL) is a close second to the Sea of Okhotsk for having the southernmost sea ice in the northern hemisphere (Takahashi et al., 2011), and its sea ice cover has been declining in recent decades (Derksen et al., 2018). Being at the southern edge of sea ice extent means that the GSL is particularly sensitive to global warming given the drastic possibility that it eventually becomes completely ice-free year round. The entire area of the Gulf can become ice covered before the end of the severest winters, while less than a quarter of the area is ice covered by the end of mild winters, usually limited to shallow portions of the Gulf such as the Northumberland Strait. Using this threshold of a quarter of the area covered by ice of stage 4 (grey ice of 10-15 cm in thickness) or greater, the Gulf has been nearly ice-free by the end of winter six times in recorded history, with four occurrences since 2010 (as will be shown below). This suggests that climate warming may have already begun to affect sea ice duration, seasonal maximum area and volume in the Gulf, as the long term warming trend added to strong interannual variability has led to more common nearly ice-free winters. The study of the forcing thresholds responsible for similar events is not only relevant, but urgent.

In the high Arctic, predictions of seasonal sea ice outlooks often focus on the melt season and ice breakup dates for navigation and industrial activity purposes (Blockley & Peterson, 2018), and to track the progession towards the September minimum that

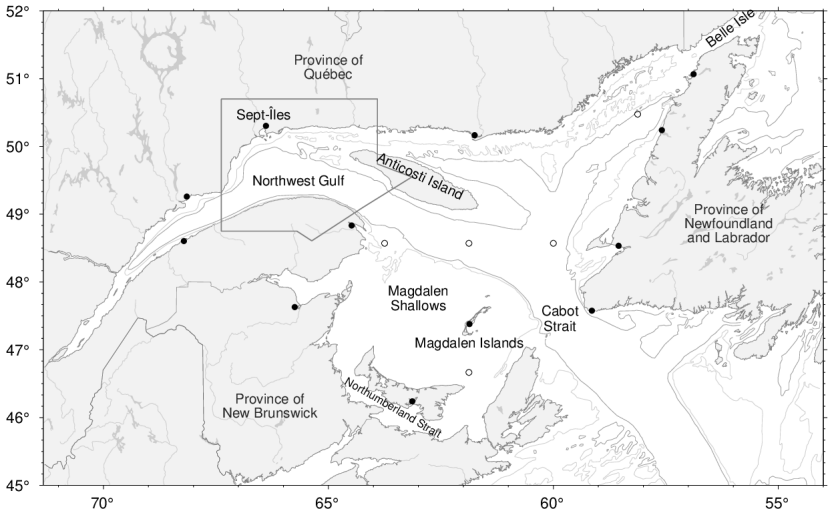

Figure 1. Gulf of St. Lawrence. Thirteen weather stations operated by Environment and Climate Change Canada (ECCC) are shown as black dots. NCEP2 grid points are shown as open circles. The area delimiting the Northwest Gulf is outlined. Isobaths for 100 m and 200 m are shown.

is expected to become ice-free on occasion within 30 to 50 years (Notz & SIMIP Community, 2020; Bonan et al., 2021). The focus is towards the opposite of forecasting the date of first occurence and of upcoming maximum sea ice conditions at lower latitudes such as the Barents Sea (Arthun et al., 2021), Greenland Sea, and the Sea of Okhotsk (Takahashi et al., 2011).

In the Gulf of St. Lawrence, the interest in seasonal forcasting lies in aid to maintaining the St. Lawrence seaway open for shipping but also to help plan tourism operations such as the observation of harp seal pups on the sea ice. These observations require sea ice floes of sufficiently large size and thickness to safely land a helicopter with tourists. One major such tourism operator reports cancelling five seasons between 2010 and 2023 because of weak sea ice conditions. Climate predictions are of interest to know when the Gulf will become completely ice-free. The topic of inter-annual variability of sea ice in the Gulf of St. Lawrence and its relationship to atmospheric forcing and initial ocean state was examined three decades ago using statistical analysis (Déry, 1992), numerical modelling (DeTracey, 1993), and a combination of both (Li, 2000) in studies that pre-dated the four recent nearly ice-free winters. Li (2000) found that observations of inter-annual variability in December to April surface air temperature accounted for 40% of the variance in sea ice area, but did not provide the linear relationship. Based on the coupled ice-ocean numerical model of Saucier et al. (2003), Senneville and Saucier (2007) found that an increase in winter air temperature of 2°C resulted in a forecasted reduction of 28% in area and 55% in volume of sea ice relative to the period 1996-2003. More recent numerical modelling has also been used to predict sea ice cover under various climate change scenarios. Brickman et al. (2016) and Lavoie et al. (2020) show maps of projected average conditions, but do not delve into the details of the relationship to atmospheric forcing; Brickman et al. (2016) model a nearly ice free Gulf by 2075 under RCP8.5 forcing, while Lavoie et al. (2020) reach the same conditions by 2061-2080 under RCP8.5 forcing for two of three Earth System Models used for atmospheric downscaling. Long et al. (2016) obtained a crossing of the interannual mean sea ice conditions through zero by 2069 with the increase in winter air temperature of 2 to 3°C. Opera-

tional models are also used for sea ice forecasting in the Gulf on the time scale of days (Pellerin et al., 2004; Smith et al., 2013).

Sea ice production is related to ocean mixed layer dynamics and to winter atmospheric conditions (air temperature, winds). The more dominant factor regionally depends on the heat content within the mixed layer, and therefore also its depth, versus the strength of the ocean-atmosphere heat flux. The summertime water column in the Gulf of St. Lawrence consists of three distinct layers: the surface layer, the cold intermediate layer (CIL), and the deeper water layer. Surface temperatures typically reach maximum values in early to mid-August (Galbraith et al., 2012). Gradual cooling occurs thereafter, and wind-forced mixing during the fall leads to a progressively deeper and colder mixed layer, eventually encompassing the CIL. During winter, the surface layer thickens partly due to buoyancy losses (cooling and reduced runoff) and brine rejection associated with sea ice formation, but mostly due to wind-driven mixing prior to ice formation (Galbraith, 2006). The surface winter layer extends to an average depth of 75 m, but may reach >150 m in places such as the Mécatina Trough where near-freezing waters from the Labrador Shelf entering through the Strait of Belle Isle may extend from the surface to the bottom, in depths >200 m (Galbraith, 2006; Shaw & Galbraith, 2023). This winter mixed layer depth is greater than values in most of the Arctic, comparable to the Eurasian Basin, but less than half that of the Barents Sea (Peralta-Ferriz & Woodgate, 2015) or the Labrador Shelf as jugded from the summer Cold Intermediate layer thickness (Cyr et al., 2022). This mixed layer must entirely reach near-freezing temperatures for sea ice to be produced, favoring sea ice formation first in shallow areas where the mixed layer reaches the bottom, or in the Estuary where the stratification limits the mixed layer to shallow depths, and suggesting that ocean heat content should play a large role in seasonal sea ice variability because of the large mixed layer depth and warm fall conditions compared to the Arctic. Restratification occurs in spring with sea ice melt waters and continental runoff lowering surface salinity, combined with surface warming. Underneath this surface layer, cold waters from the previous winter become partly insulated from the atmosphere and form the summer CIL. This layer persists until the next winter, gradually warming up and deepening during summer (Gilbert & Pettigrew, 1997; Cyr et al., 2011), and more rapidly during the fall as vertical mixing intensifies. The deep layer underneath is mostly unaffected by seasonal exchanges with the atmosphere and is not considered here since it is not involved in sea ice production.

The factors affecting the presence of sea ice in Gulf of St. Lawrence differ from the neighboring Newfoundland Shelf where the sea ice cover is mostly advected from the Labrador Shelf via the inshore branch of the Labrador Current (Prinsenberg et al., 1997; Peterson et al., 2015). Cyr et al. (2022) also found that winter air temperature measured on the coast of Labrador (Cartwright NL) does not correlate well with sea ice severity offshore, but rather with the ice metrics on the Newfoundland Shelf to the South (R^2 = 0.64 to 0.80). The effects of atmospheric circulation patterns are often difficult to differentiate, affecting both dynamics (drift) and thermodynamics (air temperature anomalies). Deser et al. (2002) considered both effects and found winter-to-winter persistence of sea ice on the Newfoundland and Labrador Shelf may be mostly driven by thermodynamics. By contrast, the case of the Gulf of St. Lawrence is simpler as it is closed off to the North and, except for limited inflow through the Strait of Belle Isle, sea ice is limited to local formation within the Gulf. This work therefore addresses thermodynamics and whether the interannual sea ice variability in the Gulf of St. Lawrence is driven by the atmosphere or by pre-existing conditions of the ocean. This work first analyses sea ice data to provide climatologies of sea ice phenology and time series of sea ice season duration and maximum estimated volume and area. It analyses winter hydrographic data to show the mixed layer conditions present during extreme cases of sea ice cover, and fall hydrographic data to determine if early-fall mixed layer conditions explain the variability. The Gulf of St. Lawrence is a rare case study for which the water column under an ice-covered sea is sampled at the end of winter, permitting the evaluation of the

mixed layer thickness that had to be cooled to near-freezing before sea ice could be produced. The work briefly considers how far ahead in time upcoming seasonal ice conditions can be forecasted. It identifies relationships between winter atmospheric forcing and observed seasonal extreme sea ice conditions, and seeks to determine if these relationships can be used to infer changes expected from future climate scenarios.

2 Materials and Methods

Ice cover area, duration, and volume are estimated from ice cover products obtained from the Canadian Ice Service (CIS), and further processed onto a regular grid used in analyses. These are weekly charts covering the period 1969-2024 downloaded from the CIS in a Geographic Information System (GIS) format. All charts are then gridded on a 0.01° latitude by 0.015° longitude grid (approximately 1 km resolution). Following Table 3.1 of the Canadian Ice Service (2005) documentation, thickness (and therefore volume) is estimated from the mean thickness of stages of ice growth whether it is new ice (stage 1, <10 cm: 5 cm), nilas (stage 2, <10 cm): 5 cm), grey ice (stage 4, 10-15 cm: 12.5 cm), grey-white ice (stage 5, 15-30 cm: 22.5 cm), thin first-year ice (stage 7, 30-70 cm: 50 cm), medium first-year ice (stage 1•, 70-120 cm: 95 cm) and thick first-year ice (stage 4•, >120 cm: 160 cm), following a practice used by Peterson and Prinsenberg (1990) and Prinsenberg et al. (1997) and routinely used for the validation of sea ice volume production in numerical models of the Gulf of St. Lawrence (Saucier et al., 2003; Tang et al., 2008; Brickman & Drozdowski, 2012; Urrego-Blanco & Sheng, 2014; Smith et al., 2013; Brickman et al., 2016). Prior to 1983, the CIS reported ice categories into fewer classifications using a single category of first-year ice ($\geq$ 30 cm) with a suggested average thickness of 65 cm. This value was found to underestimate the seasonal maximum thickness and volume based on high inter-annual correlations obtained between the estimated volume and area of the weekly seasonal maxima. The comparison of linear regressions between areas and volumes pre- and post-1983 provided an estimate of 85 cm, which is used instead of 65 cm. The reader is cautioned that volumes thus calculated are only estimates. While the practice is better suited to the finer grained categories of younger and thinner sea ice found in the Gulf of St. Lawrence than in more northern areas, the association of a standard thickness to each ice growth stage does not account well for rafting and ice charts do not account for ridging. Volumes are used here to compare relative sea ice severity.

The surface layer temperature conditions of the Gulf are monitored by complementary methods. First, three high-resolution satellite-based products are blended to produce weekly composites that cover the area from 1982 to 2024 (Galbraith et al., 2021, 2023). Second, to extend coverage during the sea ice season, a shipboard thermosalinograph consisting of temperature-salinity sensors (SBE-21; Sea-Bird Electronics Inc., Bellevue, WA) has been installed on various commercial ships of Oceanex Inc. since late 1999 (Galbraith et al., 2002). These ships transit between Montréal (Qc) and St. John's (NL) with weekly return trips, crossing the Gulf each time.

Heat flux data and daily surface air temperature were extracted from the NCEP Reanalysis 2 open dataset, provided by the NOAA/OAR/ESRL Physical Sciences Laboratory (Boulder, Colorado, USA) for 1990 to March 2024 (Kanamitsu et al., 2002).

Air temperatures come from the 2024 version of the third generation of homogenized surface air temperature dataset, which is part of the Adjusted and Homogenized Canadian Climate Data (AHCCD), and accounts for shifts due to the relocation of stations, changes in observing practices, and automation (Vincent et al., 2020). Air temperature data for 2024 were extracted from Environment Canada's National Climate Data and Information Archive (NCDIA). Thirteen coastal stations located around the Gulf are used (Figure 1). Monthly temperature climatologies are computed at each station for the period 1991-2020, and then averaged to obtain a spatial average seasonal cycle for the Gulf. Gulf average monthly air temperature anomalies are computed as the av-

erage anomalies at all available stations, and seasonal (DJF or DJFM) anomalies are computed as the average of these Gulf average monthly anomalies.

Fall water column temperature and salinity conditions were obtained from Fisheries and Oceans Canada Atlantic Zone Monitoring Program (AZMP) fall surveys (Therriault et al., 1998; Galbraith et al., 2023) using a Sea-Bird Electronics SBE-9/11 CTD probe. The survey dates have shifted from early December to mid-October/mid-November starting in 2002.

Winter mixed layer conditions have been sampled at the end of winter, in the first half of March, since 1996 using a helicopter-based oceanographic survey that is now also part of the AZMP. During these operations, a Sea-Bird Electronics SBE 19plus is lowered from the air to 200 m depth (or the sea floor in shallower areas) while the helicopter maintains a stationary flight, or through an augered ice hole once the aircraft lands on the ice. The first nine years of data collected from these surveys are described in Galbraith (2006), and 29 years of data (1996-2024) are used here. This is the first time that measured winter mixed layer heat content values are published for the Gulf.

3 Sea ice metrics climatology and interannual variability

Weekly ice charts were used to grid the day-of-year (DOY) of the first and last ice occurrences for each season, as well as the duration defined by the number of weeks that sea ice is observed at a grid point. Figure 2 shows the WMO standard 30-year climatology for these metrics, from 1991 to 2020 (WMO, 2017). Ice typically forms first in December in the upper Estuary, on the banks of the St. Lawrence Estuary, and in shallow waters along New Brunswick, Prince Edward Island, and the lower north shores. It melts last in the northeast Gulf where the ice season duration tends to be longest, apart from shallow bays elsewhere. Offshore sea ice is typically produced in the northern parts of the Gulf and drifts towards the Magdalen Islands and Cabot Strait during the ice season (Saucier et al., 2003; Urrego-Blanco & Sheng, 2014).

Figure 3 shows the 1991-2020 climatology of ice thickness distribution during the week of maximum seasonal estimated volume, as well as the maximum weekly cover observed in 2003, 2016 and 2010; 2003 is the year of maximum estimated volume and area over the 1969-2024 period, 2010 was nearly ice-free and had the warmest March mixed layer, and 2016 is a threshold year discussed later. It also shows the winter surface mixed layer temperature and depth for the same years obtained from the March oceanographic surveys (discussed later). Figure 4 presents the time series of seasonal maximum estimated ice volume, area (excluding thin new ice), and ice season duration in relation to the December to March air temperature anomaly. Ice season duration is calculated from the average of grid points shown in Figure 2, with zeros included when there is no ice in a given year but some are found in the 30-year climatology. The figure shows co-variation of sea ice metrics, a general decreasing trend since the early 1990s interrupted by strong rebounds every 5 to 6 years, and increased frequency of variability since the 1990s.

As demonstrated by these two figures, sea ice cover can vary from an almost complete cover shore-to-shore to almost no cover at all, and is tied to mixed layer conditions as surface waters have to reach freezing temperatures throughout the entire mixed layer depth to permit sea ice formation. The total area of the Gulf represents 220 000 km^2 and this area of sea ice is reached during the most severe winters (Note that the area in Fig. 4 includes drift onto the Scotian Shelf). For the purpose of this work, we define a "nearly ice free" Gulf as a maximum seasonal area of less than 1/4 of this value, although the estimated volumes will be less than a quarter than in severe winters because the ice will also be thinner during mild winters. This criterion selects 1969, 2010, 2011, 2021 and 2024 in our dataset as nearly ice free, with 2024 the record low.

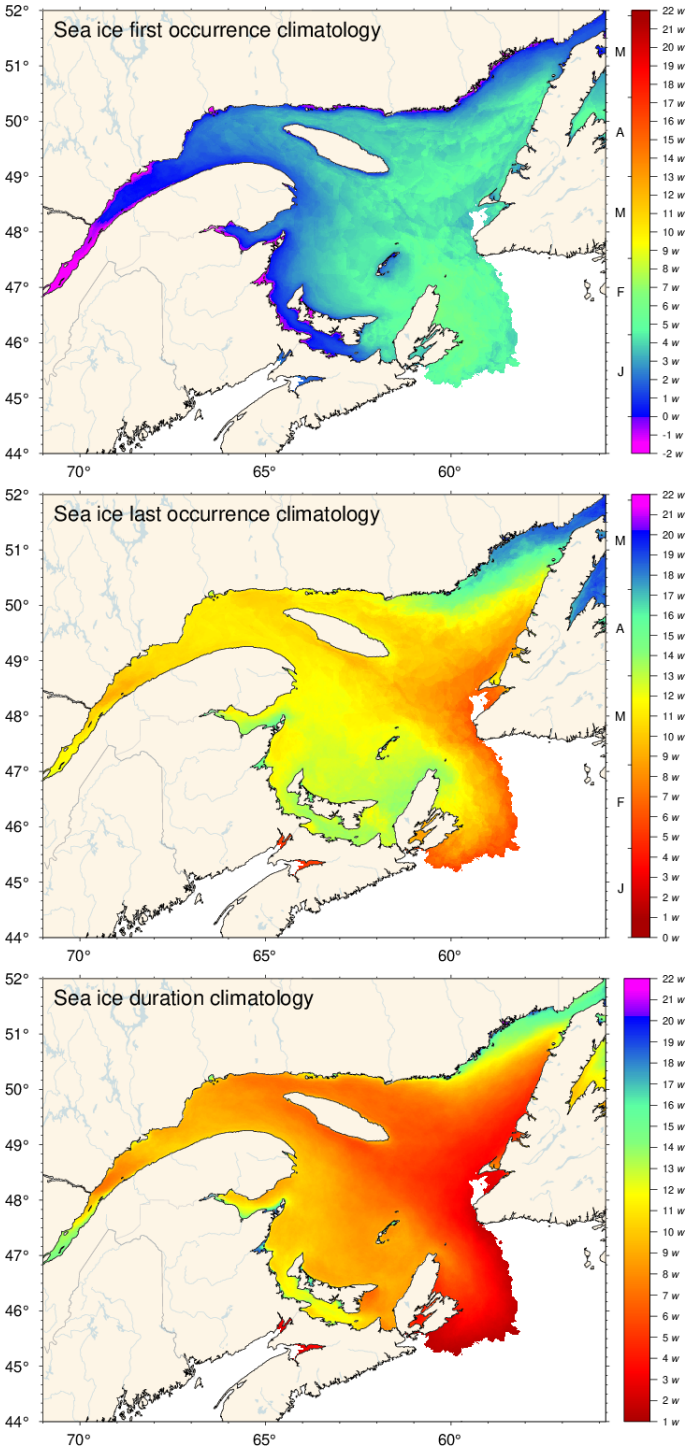

Figure 2. Sea ice phenology climatologies (1991-2020) for the first and last ice occurrence, and ice season duration based on weekly data. The first and last occurrences are defined here as the first and last weekly chart in which any amount of ice is recorded for each pixel, and are shown as day-of-year (DOY). Ice duration sums the number of weeks with ice cover for each pixel. Climatology is shown for pixels with at least 15 of the 30 years with sea ice, and therefore also displays the area where there is 50% probability of having sea ice for at least one week in a given year.

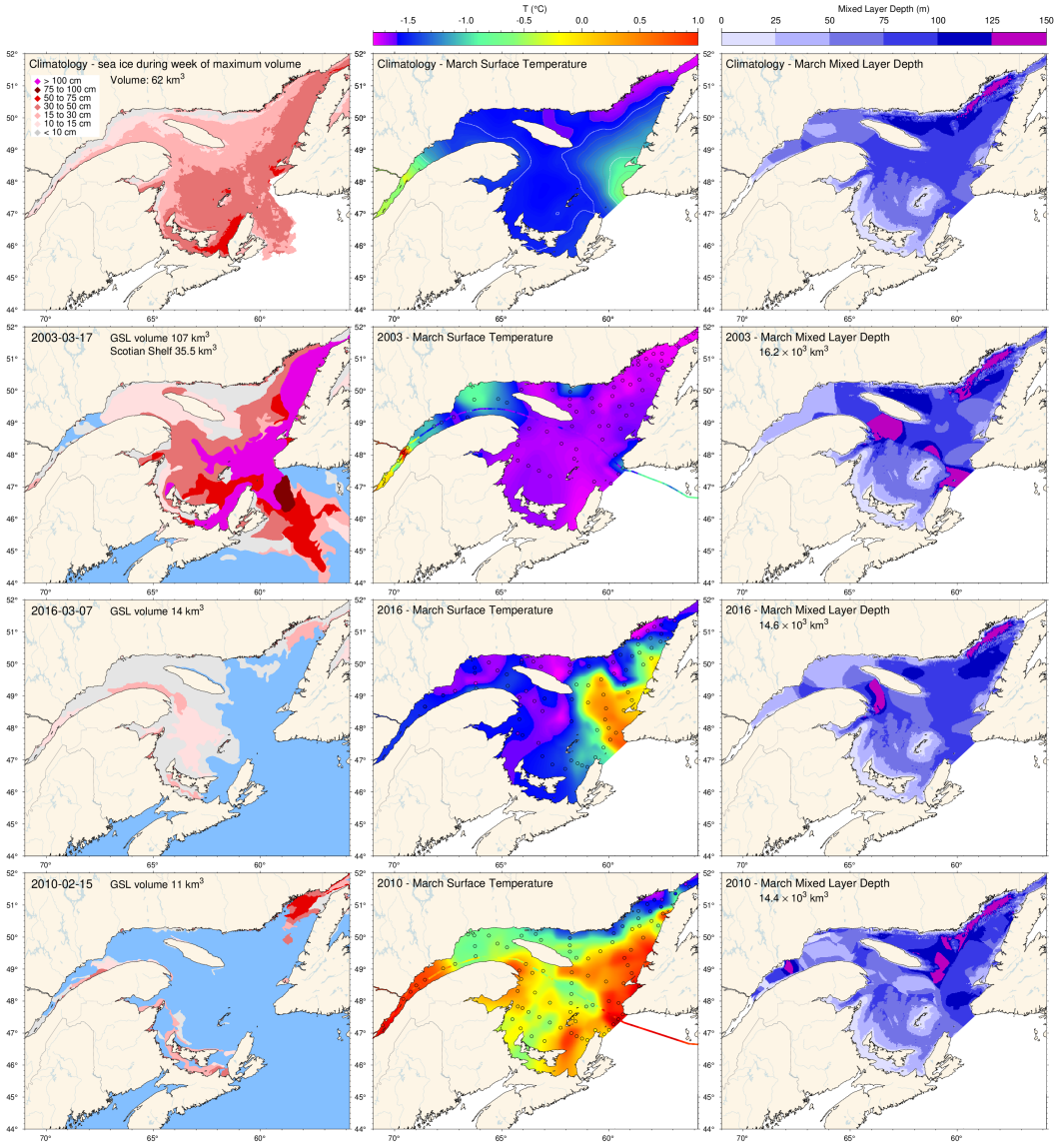

Figure 3. Sea ice thickness distribution during week of maximum seasonal estimated volume, sea surface temperature and mixed layer depth during the early March survey. On the left panels, sea ice thickness for the 1991-2020 climatology, and years 2003 (year of maximum estimated volume or area), 2016 (threshold year), and 2010 (year of largest March mixed layer heat content). On the middle panels, sea surface temperature interpolated from March survey stations for the 1996-2020 climatology and years 2003, 2016, and 2010, with station locations indicated by circles on the annual maps. Circles are color-coded according to observed temperature and a shipboard thermosalinograph transect is superimposed on the 2003 and 2010 maps. On the right panels, mixed layer depth interpolated from March survey stations for the 1996-2020 climatology and years 2003, 2016, and 2010. Integrated volumes are indicated.

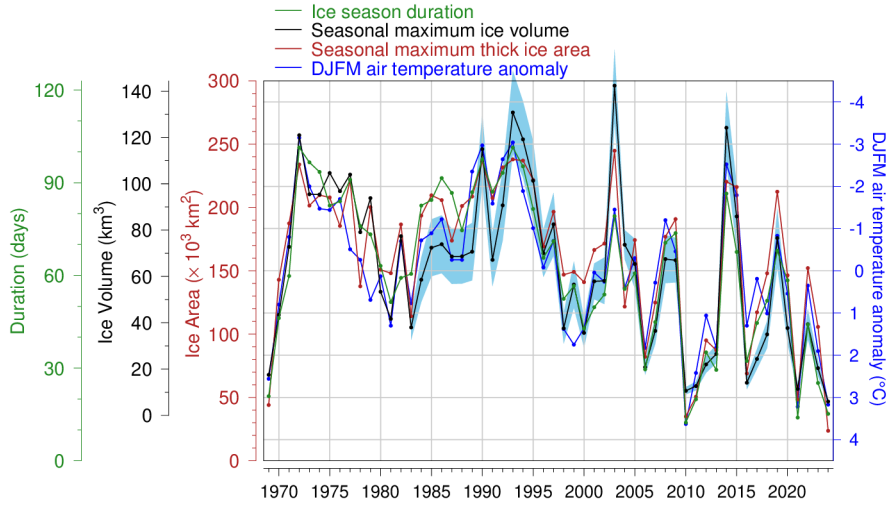

Figure 4. Seasonal maximum ice estimated volume and area including the portion on the Scotian Shelf (area excludes ice less than 10 cm thick), ice season duration, and December to March air temperature anomaly (reversed scale). Mean duration obtained as the spatial average of Fig. 2, excluding the Scotian Shelf, with zeros counted if no ice is present but the 1991-2020 climatology has some. The blue shading represents the uncertainty of estimated volumes (1983 and later) associated with the range of thickness attributed to each ice growth stage, using 25% and 75% of the thickness range as lower and upper bounds. Linear relations indicate losses of 18 km^3, 32 000 km^2 and 14 days of the sea ice season for each 1°C increase in winter air temperature (R^2 of 0.76, 0.82, and 0.84 respectively).

In 2010, the mixed layer failed to reach near-freezing by early March everywhere except close to the Strait of Belle Isle, preventing widespread sea ice occurrence (Fig. 3). This contrasts with 2003 when the mixed layer was near-freezing over the entire Gulf area in early March. The climatology shows an area near the Eastern end of Cabot Strait where waters are often warmer than freezing; this is an area often devoid of sea ice, such as in 2016. The size of this warm area is highly variable from year-to-year, extending north past the tip of Anticosti Island in 2016. The nearshore zone of the Eastern end of Cabot Strait remains ice-free in the climatology (top left panel), indicating open water conditions during at least 50% of winters.

4 Relation to fall ocean heat content

Since the fall mixed layer temperature must reach the freezing point before sea ice can form, the fall heat content was hypothesized to be decisive for the date of the first occurrence of sea ice in the Gulf of St. Lawrence. The fall oceanographic survey carried out by Fisheries and Oceans Canada was historically called the *ice forecast cruise*, when it was usually carried out in December. In the 1990s, collected temperature-salinity profiles were sent to the Canadian Ice Service for comparison to prior years of observations to serve as input for the seasonal sea ice outlook. This nickname has remained even though the survey has usually been conducted in October for the past 20 years or so. With the benefit of hindsight, this hypothesis can and is hereby tested.

To test whether the fall heat content obtained from surveys conducted in December (before 2002) and October (after and including 2002) has any predictive ability for the first appearance of sea ice, the mixed layer depth measured at each station for each

March sampling was first interpolated over the area of the Gulf using the Barnes algorithm as in Galbraith (2006) (e.g. Figure 3). The mixed layer depth is defined here as the depth where salinity is 0.3 greater than the deepest water with $T < -1°C$, or of the coldest water if no waters with $T < -1°C$ are present (which occurs throughout the Gulf in 2010). The addition of 0.3 only serves to extend the mixed layer to the sharp halocline usually present beneath the mixed layer and the ad hoc value of 0.3 is not consequential to the results. The mixed layer depth was then integrated horizontally, providing the mixed layer volume whose heat content was estimated referenced to the freezing point, as a function of the interpolated value of surface salinity. In the following, the heat content will be displayed in ExaJoules (EJ or $\times 10^{18}$ J) and in units of $km^3\,°C$ for simplicity, omitting negligible variations of density and specific heat capacity of water. Finally, the March mixed layer depth grid was transposed to the preceding fall observations and the fall heat content was calculated over the same volume.

The average day-of-year of the first ice occurrence cannot be calculated with a simple average of seasonal grids such as in Figure 2. This would lead to biased estimates due to spatial disparity in the date of first occurrence and interannual variability in sea ice extent; e.g., the sea ice cover extends further out to Eastern Cabot Strait in winters of high sea ice, where the first occurrence is later. Instead, the spatial anomaly grid was calculated for each ice season, relative to the 1991-2020 climatology of the first occurrence, and the spatial average anomaly obtained from this grid is used. Figure 5 (top panel) shows the time series for the average anomaly of first ice occurrence for 1996-2024 and the heat content of the previous fall, i.e. 1995-2023. No statistical relationship is found between these two series, either using the full sequences or excluding 1996-2002 when the preceding fall survey was done in December (R^2 of 0.08 and 0.06 respectively), or even using the short series of 1996-2002. The fall heat content has a statistically significant warming trend but the day-of-year of first occurrence just barely has a trend to later occurences. Furthermore, the two years with the latest first sea ice occurrence (2021 and 2011) did not follow a high fall heat content (although the 3rd, 2023, did) nor did the three post-2002 years with the earliest first occurrence (2014, 2019 and 2009) coincide with winters following low fall heat content (2006, 2018 and 2003).

Next, the predictive ability of the fall heat content for the winter mixed layer volume and heat content, or for the maximum seasonal estimated ice volume was tested (Figure 5, bottom panel). Again, the fall heat content is not statistically related to any of these three parameters. Winters 2010 and 2021, which show low sea ice cover and high remaining heat content in March, were both preceded by near-average fall heat content. Winters 2003 and 2014, which are characterized by more sea ice and lower winter mixed layer heat content than average, were also preceded by near-average fall heat content. The exceptionally high fall heat content that preceeded winter 2022 did not coincide with high March heat content or record low sea ice estimated volume. Figure 5 also shows that the interannual variability in the heat content of the March surface mixed layer is not driven by differences in its volume, the two being weakly correlated.

5 Sea surface temperature coupling to air temperature

Galbraith et al. (2012) showed that the May-to-November monthly climatology of sea surface temperature averaged over the Gulf of St. Lawrence was nearly identical to that of air temperature lagged by half a month. This is shown in Figure 6 using updated datasets and climatology, which here covers the period 1991-2020. From spring to the seasonal maximum sea surface temperature in August, the atmosphere remains warmer than the surface waters and warms them. The opposite occurs once the seasonal maximum is reached when the atmosphere becomes cooler and cools them. This tight interrelation, at least in a climatological sense, informs on the role played by the sensible heat flux, which is a first-order mechanism affecting surface conditions. The sensible heat flux can be estimated by the bulk aerodynamic formulae $Q_s = \rho_a C_{pa} C_H |U|(\mathrm{SST} - T_a)$, where

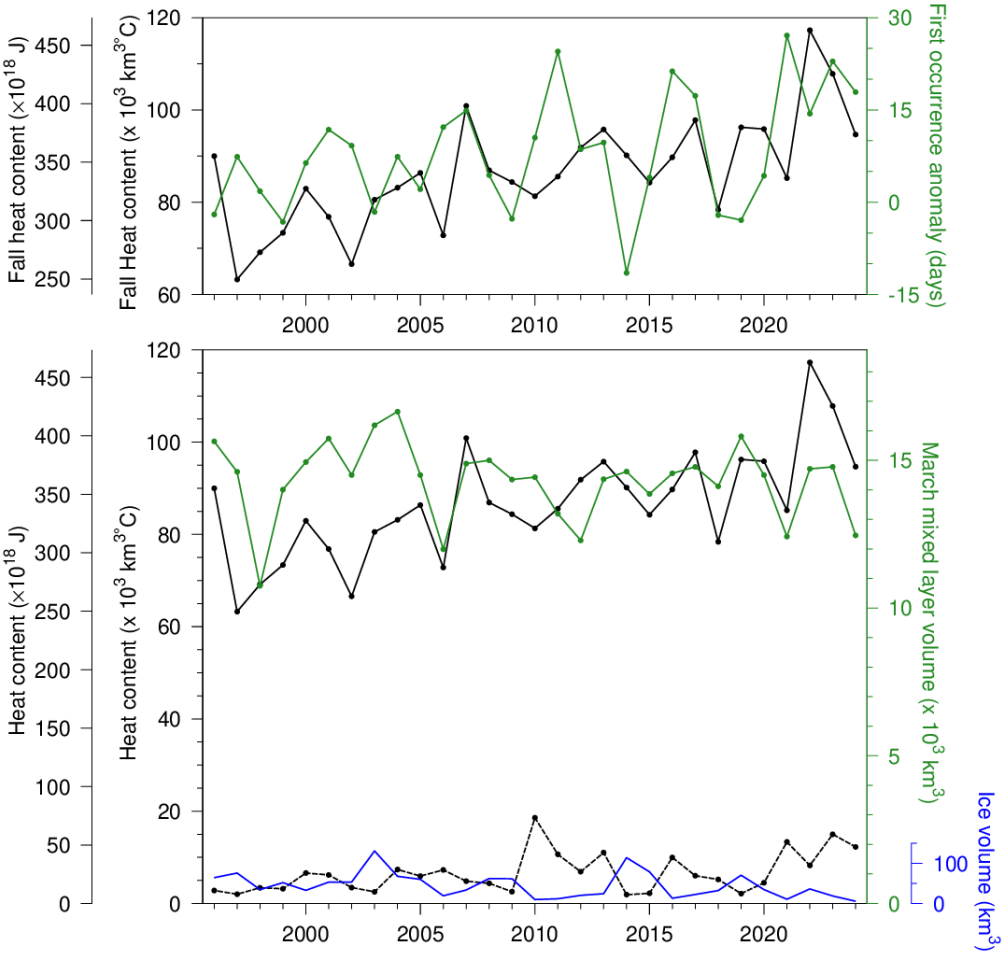

Figure 5. Heat content in the Gulf of St. Lawrence. (Top) Heat content observed during the fall oceanographic survey in the volume occupied by the following March surface mixed layer (black line) and the spatial average of the day of the first occurrence of sea ice anomaly grid (green line). Years are referenced to March (i.e. Fall 2020 is shown at 2021). (Bottom) Same fall heat content as above (black line) compared to March mixed layer volume ($T < 0$°C; green line), March surface mixed layer heat content (black dashed line), and the heat removed for the formation of the maximum observed weekly estimated volume of sea ice (blue line). Ice volume is scaled according to the latent heat of fusion required for its formation.

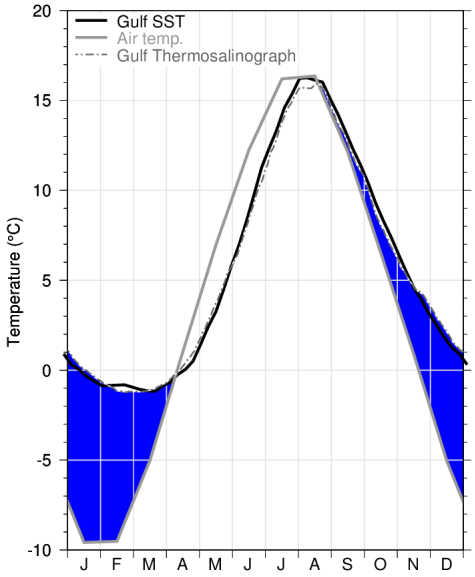

Figure 6. Sea surface and air temperature climatological seasonal cycle in the Gulf of St. Lawrence. AVHRR temperature weekly averages for 1991-2020 are shown (thick black line) as well as thermosalinograph averages (2000-2020; gray dashed line) and monthly air temperature averaged over 13 stations in the Gulf of St. Lawrence for 1991-2020 (thick gray line). The area in blue highlights water and air temperature differences when air is colder than water. See Figure 1 for weather station locations.

ρ_a is the air density, C_{pa} is the specific heat of air, C_H is the sensible heat transfer coefficient (e.g. MacIntyre et al., 2002) and U is the wind velocity. Since it is proportional to air and water temperature difference, it increases as the air gets warmer than surface waters in spring, and, at some temperature difference given average wind speeds, may become large enough to warm the surface waters at the same rate as the air temperature and to maintain a nearly constant near-surface temperature difference. This is in spite of sensible heat flux being a smaller contribution to the overall heat budget than solar radiation during the summer season. The reverse same situation occurs in the fall except that the mixed layer thickens as the season progresses, increasing the required heat flux to reach equilibium and therefore the temperature difference between air and water. Galbraith et al. (2012) have shown that this strong coupling holds interannually, with the April-November Gulf average air temperature correlated with the May-November sea surface temperature (1982-2010). An analysis using the updated time series over the years 1982 to 2023 finds that the two are correlated with $R^2 = 0.75$.

This strong coupling is likely responsible for the low correlation between fall water column heat content and either the timing of the onset of sea ice, the maximum estimated volume of sea ice formed, or the remaining water column heat content in March. Whatever the initial fall heat content within the water column might be, the ocean surface temperature generally follows the air temperature with a half-month lag: it remains well above freezing if the air temperature stays anomalously warm, or cools rapidly if air temperature cools rapidly. When air temperatures fall below freezing, with water temperature bound by its freezing point, the temperature difference and sensible heat flux both increase to reach values much greater than observed in other seasons. Therefore the timing of the first sea ice occurrence (and subsequent sea ice and winter mixed layer conditions) is only expected to be influenced by the date at which the air temperature

falls below the freezing point of seawater, triggering sea ice production, rather than by the warmer air temperature experienced the previous fall. To partly demonstrate this, the relations are explored between the DOY of when air temperature and SST reach various thresholds in the Northwest Gulf with the DOY of the first sea ice occurrence.

Figure 7 shows the comparison between the DOY of the first ice occurrence in the Northwest Gulf and the DOY when SST averaged within the region reaches below various temperature thresholds, based on twice weekly shipborne thermosalinograph transects (see the delimitation of the Northwest Gulf area in Figure 1). The very first occurrence of sea ice is defined firstly as the estimated volume within the region crossing the threshold of 5% of the largest estimated volume ever recorded in the region and secondly as the spatially averaged DOY of first occurrence, i.e. the spatial average of the DOY anomaly of the first ice occurrence at all grid points in the region in Fig. 2 added to the climatological average value of the region. Very first occurrence occurs on average on DOY 13 (2001-2024) and the spatial average occurs on DOY 20. Time series are not detrended prior to correlations on the assumption that a trend to warmer air temperature or SST would in fact be part of the variance that would cause later ice formation. Correlations coefficients against the DOY of SST reaching low temperatures are highest at near-freezing temperatures for which the time lag is very short (about one week for SST of -1°C with the spatial average of ice first occurrence and simultaneously with very first occurrence) and decrease almost linearly with increasing threshold temperature, with lead time also increasing almost linearly. The timing of SST dipping below 0°C is a very strong predictor of sea ice; it explains 73% of the variance of the very first occurrence of sea ice with an average lead time of 17 days, and 79% of the spatial average of first occurrence with an average lead time of 24 days. The DOY of SST crossing 1°C is still a useful predictor at $R^2 = 0.5$, with an average lead time of 30 days for very first ice occurrence and of 37 days for the average first ice occurrence.

The next step is the link to air temperature. The same DOY time series for first occurrence of sea ice are compared in Figure 7 to the DOY for air temperature at 2 m dipping below thresholds of 3 to -6°C at the NCEP grid point closest to the Northwest Gulf area. The NCEP air temperature time series was first filtered with a 15-day moving average. Using air temperature as a predictor introduces another step in the process, increasing lead time but decreasing the statistical reliability somewhat. The air temperature thresholds of -5°C to -2°C lead to similar coefficients of determination ($R^2 = 0.47$ to 0.61) with lead times of 37 to 44 days at -2°C; 7 days more than using SST at 1°C with a similar coefficient of determination. The air temperature threshold of -6°C leads to reduced correlations because during some years the air temperature stagnates between -5°C and -6°C. Higher air temperature crossings up to 0°C are less statistically powerful predictors ($R^2 = 0.29$ to 0.38) with a lead time of 49 to 56 days. As hypothesized above, air temperature crossing below thresholds of 1°C and warmer have reduced predictive power.

6 Predictibility of seasonal maximum from past conditions

If the onset of sea ice can only be statistically predicted from SST or air temperature with lead times of up to 37 to 44 days, how far ahead of time can the severity of the seasonal maximum be predicted from sea ice observations that preceed it? Fig. 7 (bottom panel) shows the correlation coefficients between the seasonal maximum of sea ice area (stage 4 or greater) and of estimated volume against the measured quantity at a given prior date for all recorded seasons (1969-2024). In this analysis, the area/volume time series are converted to monotonically increasing, meaning that decreases during the season are not considered and prior higher values are held.

The area reaches its seasonal maximum at the median DOY of 58 and can be predicted with R^2=0.5 from the area measured on DOY 22, a lead time of 36 days. The es-

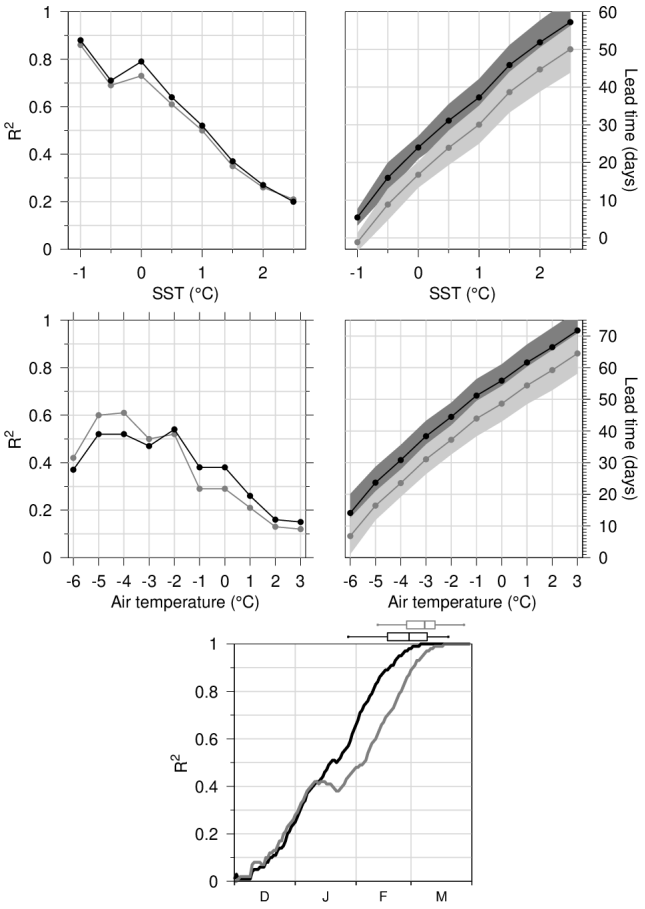

Figure 7. Analysis of sea ice predictibility in the Gulf of St. Lawrence. The top four panel are for first occurrence of sea ice in the Northwestern Gulf. (Left panels) Coefficients of determination (R^2) between time series of first occurrence of ice and of the DOY of SST (top) and of air temperature (bottom) cooling below threshold temperatures, and (right panels) time lag with first occurrence of ice (plus and minus half the standard deviation as grayed area, partially hidden). The SST is based on twice weekly shipborne thermosalinograph transects (2001-2024, excl. 2010, 2014, and 2015 for which there are no SST data within the time range). First occurrence of ice is from two methods: (gray lines) very first occurrence is defined as the DOY when the estimated volume reaches 5% of the largest estimated volume ever recorded in the region (Figure 27 of Galbraith et al. (2023)), and (black lines) the spatial average of first occurrence of ice defined as the average anomaly at every grid point of maps such as in Fig. 2 plus the climatological mean in the area delimited as in Figure 1. The air temperature is from the closest NCEP grid point, with a 15-day moving average applied to the air temperature time series. (Bottom panel) Predictibility of the seasonal maximum estimated sea ice volume (grey line) and area (stage 4 or greater; black line) as a function of the maximum measured quantity at a given prior date (1969-2024). The box plots show the statistics of the timing of the seasonal maximums of estimated volume and area.

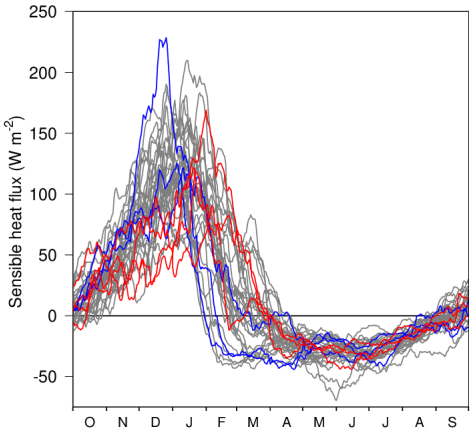

Figure 8. Sensible heat net flux from the NCEP/DOE AMIP-II Reanalysis (Reanalysis-2) with daily averages of 5 grid points in the Gulf of St. Lawrence, filtered using a 31-day running mean (1990-2024). Years are shown from October to October to highlight the winter mixed layer formation period. Years with the highest maximum seasonal estimated ice volume (2003, 1993, and 2014) are shown in blue, years with the lowest maximum seasonal estimated ice volume (2024, 2010, 2021, and 2011) are shown in red, and all others are in gray.

timated volume reaches its sesonal maximum at the median DOY of 65 and can be predicted with R^2=0.5 from the volume estimated on DOY 36, a lead time of 29 days.

7 Sea ice conditions and their relation to winter air temperature

Sea ice production is related to winter atmospheric conditions (air temperature, winds) and ocean mixed layer dynamics. As stated earlier, the striking similarity between May-November surface air temperature and SST suggests a tight coupling through sensible heat flux. This coupling must intensify when air temperatures drop below the freezing point of sea water, increasing the air-sea temperature difference and sensible heat flux. Fig 8 displays the net sensible heat flux extracted from the NCEP dataset and averaged over the five grid points covering the Gulf of St. Lawrence. On average, sensible heat flux accounts for about half of the heat budget in January (100 W versus 200 W), with latent heat flux accounting for most of the remainder. Sensible heat flux decreases quickly in February, more so in high sea ice years (shown in blue) than in low ice years (shown in red) because of the limited area of open water. Surprisingly, this data set shows sensible heat flux becoming negative as early as the end of January in 1993 (blue line with the earliest crossing to negative values) in spite of air temperatures in February 1993 being 5.3°C below the 1991-2020 climatology (and the third coldest month of February on record since 1873, with the coldest being 1923 and 1914 with 6.3 and 5.9 °C below the 1991-2020 climatology, respectively).

In order to find the simplest descriptor of the integrated heat flux variability that can affect the formation of the winter mixed layer and sea ice cover, the blue shaded area in Fig. 6 was investigated, i.e. when the air temperature is colder than water temperature in the climatology. Because SST is close to 0°C between December and March, when the air-water temperature difference is largest, the area in blue representing the air-water temperature difference intrinsic to the sensible heat flux is well approximated by the average winter air temperature (DJFM). This metric is shown in Fig. 4 (blue line) and is highly correlated with all sea ice metrics, with R^2 values ranging from 0.76 to 0.84.

8 Discussion and summary

The spring-to-summer sea surface temperature averaged over the Gulf of St. Lawrence is similar to that of air temperature lagged by a half-month, suggesting strong coupling between the two through sensible heat flux. Perhaps counter-intuitively, because of this strong coupling, the early fall heat content in the volume that will eventually become occupied by the winter mixed layer is not an important driver of the date of the first occurrence of sea ice in the Gulf of St. Lawrence. Only the time period when air and water temperature get close to freezing is decisive. The very first and average first occurrences of sea ice were shown to occur about 17 and 24 days, respectively, after SST reaches an average of 0°C in the Northwest Gulf (R^2 = 0.73-0.79), and 30 and 37 days after it reaches 1°C (R^2 = 0.5). Using air temperature crossing -2°C as a predictor can increase the lead time by 7 days to 37 and 44 days with similar confidence, at R^2 = 0.47-0.61 (Figure 7).

Figure 9 shows the correlation coefficient of determination (R^2) matrix between various sea ice seasonal maximum and duration metrics against air temperature in the Gulf of St. Lawrence. Although correlation statistics should be done using time series that have have been detrended if outside factors may cause trends that would cause spurious correlation, here trends in sea ice metrics can be assumed to be caused by a warming trend. This is supported by trends in durations, areas and estimated volumes that are within confidence intervals of predictions based on linear regressions with air temperature and air temperature trends. Nevertheless, correlation coefficients are also shown for detrended time series and correlations are only slightly weakened and still statistically significant. Once the surface water is limited by the freezing point, which is close to 0°C, the sensible heat flux reaches its maximum values. The average air temperature then acts as a proxy for the difference between the sea surface and air temperatures, and sea ice metrics become strongly correlated with the mean air temperature for the December to March (DJFM) period. This relationship most likely operates through the sensible heat flux. Correlations are also high (and in some cases higher) against the average air temperature observed between December and February (DJF). In years of very light sea ice cover, the maximum often occurs early, in February, making the March temperatures moot (although very cold March temperatures might have delayed the maximum). In years of very high sea ice cover, the Gulf is mostly ice-covered by March, which reduces the area over which sea-air heat flux can occur, making the March temperatures a less useful predictor of average sensible heat flux. It is therefore not surprising that the DJF average air temperature proved to be a slightly better predictor than the DJFM average air temperature for two of three sea ice parameters. In spite of reduced sensible heat fluxes often observed in February (Fig. 8), removing this month from the averaging period (leaving only December and January) leads to still statistically significant but much reduced correlations, between 0.52 and 0.76 down from between 0.75 and 0.86.

The average winter air temperature is a very good predictor of sea ice conditions metrics, with linear relations indicating losses of 18 km^3, 32 000 km^2 and 14 days of the sea ice season for each 1°C increase in DJFM air temperature (R^2 of 0.76, 0.82, and 0.84 respectively) and of 17 km^3, 31 000 km^2 and 13 days of sea ice season for each 1°C increase in DJF air temperature (R^2 of 0.75, 0.85 and 0.86 respectively). While climate change projections usually need to extrapolate outside of the observed variability to forecast near-zero conditions, the observations since 1969 include the near absence of sea ice and are thus within the bounds of interpolation.

Figure 10 shows the long-term average DJF temperature anomaly from all available meteorological stations back to 1873, when only 3 stations were available. A warming trend of 2.4°C per 100 years is observed superimposed on a high interannual variability. Only six winters had DJF temperature anomalies of 2.9°C or more in that period (the next was of 2.2°C), and DJFM temperature anomalies greater than 2.4°C (the

R^2 Table	Ice max volume (1969-2024)	Ice Duration (1969-2024)	DJFM air temp (1969-2024)	DJF air temp (1969-2024)	DJ air temp (1969-2024)
Ice max area (1969-2024)	**0.81 (0.77)**	**0.85 (0.84)**	**0.82 (0.79)**	**0.85 (0.82)**	**0.65 (0.58)**
Ice max volume (1969-2024)		**0.79 (0.74)**	**0.76 (0.72)**	**0.75 (0.69)**	**0.52 (0.42)**
Ice Duration (1969-2024)			**0.84 (0.83)**	**0.86 (0.82)**	**0.76 (0.68)**
DJFM air temp (1969-2024)				**0.93 (0.92)**	**0.69 (0.64)**
DJF air temp (1969-2024)					**0.81 (0.76)**

Figure 9. Correlation coefficients of determination (R^2) for regressions between sea ice and air temperature time series for the Gulf of St. Lawrence, in parentheses for detrended time series. All are statistically significant ($p < 0.05$; auto-correlation of the time series is not considered to reduce the number of degrees of freedom).

next was of 1.9°C), and they all coincide with the only winters that were nearly ice-free in the Gulf of St. Lawrence. These are recorded in our sea ice dataset as 1969, 2010, 2011, 2021 and 2024. To those five years is added 1958 for which sea ice was reported to extend eastward to only just East of Prince Edward Island and the Western end of Anticosti Island (Black, 1958), resembling conditions of 2021. Prior to 1958, no winters were likely to have been sufficiently warm to lead to nearly ice-free conditions in the Gulf. However, the Gulf of St. Lawrence has since entered a period with occasional nearly ice-free winters, a condition that is expected to become more common in the near future. Note that the term used here is "nearly ice-free" condition because the coastal areas and shallow bays that freeze up early (Figure 2) will likely remain at least occasionally ice-covered in spite of warming for far longer. This temperature anomaly threshold is similar to that of 2 to 4°C found for various regions of the Sea of Okhotsk by Takahashi et al. (2011), also using the correlation between winter air temperature and sea ice extent.

The more recent warming trend (1962-2024) in winter air temperatures of 3.6°C per 100 years (Figure 10) hints at being steeper than the entire series trend but is not statistically different at 95% confidence intervals. If the long term trend is maintained, winter air temperatures will reach an average of 2.4°C warmer than the 1991-2020 climatology after about 100 years; earlier if the warming rate increases as the trend over the more recent period suggests and as climate models project (see below). But even then, interannual variability in air temperature associated with weather patterns, e.g. the polar vortex, will continue to drive interannual variability in sea ice. In the early 1990s, DJF average air temperatures were about 3°C colder than the long-term trend. If colder than normal temperatures of this magnitude still occur on occasion, it might take another 100 years for the Gulf to become permanently ice-free except for coastal ice.

However, this discussion hinges on the temperature anomaly threshold that distinguishes the years with nearly no ice cover, while these years were also characterized by a winter mixed layer that was significantly warmer than required to prevent ice formation. In March 2010, for example, the mixed layer was 1°C above freezing over the Magdalen Shallows and over 2°C above freezing on the Southeastern area between the coast of Newfoundland and Anticosti Island (Figure 3). Perhaps a year such as 2016 is more relevant, when the mixed layer was overall 1°C cooler and near-freezing over the Magdalen Shallows, with sea ice that had just started to form (Figure 3). The DJF winter air temperature anomaly was then of +2.2°C (Figure 10), the next warmest after the six nearly ice-free winters, a threshold that could be reached two to three decades sooner in the long-term trend.

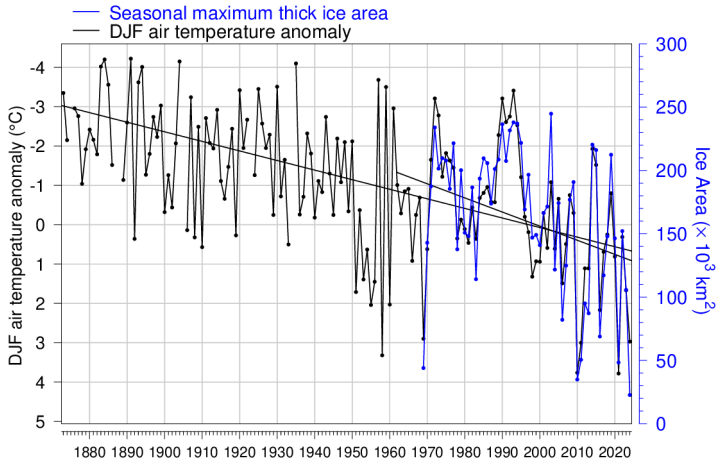

Figure 10. Seasonal maximum ice area (stage 4 and greater) and December-to-February (DJF) air temperature anomaly relative to 1991-2020 climatology, averaged over meteorological around the Gulf of St. Lawrence (reversed scale). Black lines show linear regressions for two periods. The 1873-2024 trend in air temperature is 2.4°C per 100 years and 1962-2024 is 3.6°C per 100 years but is not statistically different at 95% confidence intervals.

These projections are consistent with some aspects of recent numerical modelling results. Perrie et al. (2015) investigated the effects of IPCC SRES scenario A1B that assumes increasing carbon dioxide emissions until around 2050 and decreasing thereafter, which is a moderate emission scenario similar to RCP6.0. Using downscaling projections over the Gulf, they found winter air temperatures increases of 2.5 to 3.5°C by 2040-2069 and of 4 to 5°C by 2070-2099 relative to 1970-1999. We must reduce these increases by 0.8°C to account for our already warmer 1991-2020 climatology (based on our 13-station average time series). This is slightly faster warming than the current rate. Long et al. (2016) modelled sea ice changes in the Gulf using the same IPCC scenario and obtained a crossing of the interannual mean sea ice conditions through zero by 2069, leaving interannual variability to create some ice in colder than normal years. This is also slightly faster than the current rate but is consistent with the increase in winter air temperature of 2 to 3° averaged over the Gulf. Note that their modelled sea ice volume time series exhibits much less interannual variability than our observations and does not show the near absence of sea ice that has already occurred before the 2050s. We speculate that the relatively thin winter mixed layer in the model leads to easier production of sea ice. Indeed some numerical models obtain a sea ice cover under current climate conditions that are similar to observations, but with a much thinner winter mixed layer thickness, casting doubt on their ability to predict future climates given the assumed influence of the oceanic surface mixed layer on sea ice conditions. The winter depth of the 0°C isotherm modelled by Long et al. (2016) reaches only about 40 m in the center of the Gulf instead of the much deeper observations (see their Fig. 7). Saucier et al. (2003) also successfully simulated the sea ice cover to within error bars of observations, while simultaneously underestimating the volume of the surface mixed layer ($T < 0$°C) to only 7000 km^3, or less than half the volume typically observed (Fig. 5).

While numerical modelling can be a very useful tool to forecast sea ice conditions in the Gulf of St. Lawrence that will be associated with climate change, they currently have limitations in correctly modelling the present winter mixed layer. Therefore studies such as the present one based on understanding observations, quantifying variability, and identifying simple relations between forcings and observed conditions are com-

plementary and valuable, allowing the use of past variability to forecast conditions associated with anticipated changes in climate.

Our main result is that thermodynamics during the winter drive the sea ice cover of the Gulf of St. Lawrence, with air temperature explaining up to 85% of the maximum seasonal sea ice area. Nevertheless winds and currents do play a role. The ice cover during the record year of 2003 greatly exceeded expectations from the air temperature correlation (Figure 4) and the ice was transported out of the Gulf through Cabot Strait to a much greater extent than usual (Figure 3). This was very likely due to stronger northwesterly winds, pushing the ice southeast as it formed in the northwest Gulf and creating open water that facilitated further sea ice formation. The Gulf is charactized by persistent currents that also affect winter sea ice formation. In the Estuary, the outflowing Gaspé Current (Galbraith et al., 2023, Figure 57) transports ice out and into the Gulf, again promoting new ice formation. In the Northeast Gulf, inflow through the Strait of Belle Isle is stronger between September and February than during other months (Shaw & Galbraith, 2023), promoting some inflow of sea ice from the Labrador Shelf that contributes to the overall budget. Inflow also occurs later in the season, when the sea ice that formed in the Gulf has already melted, resulting in the later last occurrence in that area (Figure 2).

The Gulf of St. Lawrence has a winter mixed layer that is comparably thick (average of 75 m; Galbraith, 2006) with respect to typical values in the Arctic basins (Peralta-Ferriz & Woodgate, 2015). It may thus be somewhat surprising to reach the conclusion that interannual sea ice metrics are driven by atmospheric temperature variability, similarly to the Sea of Okhotsk (Takahashi et al., 2011), rather than by ocean heat content. In the Arctic Ocean, the prediction of the minimum conditions in September face what has been termed a June 1st "spring barrier" (Bonan et al., 2019) whereby the variability of onset of melt limits forecasts before that date. In the Gulf of St. Lawrence, the first occurrence of sea ice and the overall seasonal ice severity cannot be predicted by the heat content in early fall as it is lost to the atmosphere quickly enough in any case when air temperatures fall below freezing. The late fall air temperature in the Northwest Gulf predicts first occurrence of sea ice in that area with a lead time of 37-44 days after air temperature drops below -2°C, and the overall Gulf sea ice cover severity for the season (as determined by duration and by maximum area and estimated volume) are highly correlated with January-February or January-March air temperatures, yielding relations that are useful for assesments of climate change impacts (e.g. losses of 18 km^3, 31 000 km^2 and 14 days of the sea ice season for each 1°C increase in DJFM air temperature). The seasonal maximum conditions in area or estimated volume can be estimated by the preceding measurements of the same metrics with a lead time of only 29 days for volume and 36 days for area. Six nearly ice-free winters correspond to the warmest December to February (or December to March) average air temperatures over the Gulf, from which we infer a warming of > 1.9°C to 2.4°C (DJFM) or > 2.2°C to 2.9°C (DJF) above the 1991-2020 climatology leads to nearly ice-free conditions in the Gulf of St. Lawrence.

Open Research Section

Sea ice charts were downloaded from the Canadian Ice Service web site on its Archive section (https://iceweb1.cis.ec.gc.ca/Archive/page1.xhtml). Heat flux data and daily surface air temperature were extracted from the NCEP Reanalysis 2 open dataset, provided by the NOAA/OAR/ESRL Physical Sciences Laboratory (Boulder, Colorado, USA) (Kanamitsu et al., 2002) from https://psl.noaa.gov/data/gridded/data.ncep.reanalysis2.html. Monthly air temperature averages from Environment and Climate Change Canada (ECCC) (Vincent et al., 2020) and were downloaded from the Adjusted and Homogenized Canadian Climate Data (AHCCD) web site (https://open.canada.ca/data/en/dataset/fc09beda-744f-48df-ab7c-0949152e961f). Air temperature data for 2024 were extracted from Environment Canada's National Climate Data and Information Archive (NCDIA) at

https://climate.weather.gc.ca/prods_servs/cdn_climate_summary_e.html. The Ship thermograph data and the Fall and March water column temperature and salinity profiles are from Fisheries and Oceans Canada's Atlantic Zone Monitoring Program (AZMP) and are available by request to Fisheries and Oceans Canada's Marine Environmental Data at https://www.meds-sdmm.dfo-mpo.gc.ca/isdm-gdsi/request-commande/form-eng.asp. These data are in the process of being made available through the Canadian Integrated Ocean Observing System (CIOOS) web portal (https://catalogue.cioos.ca/en/).

Acknowledgments

We thank the Canadian Ice Service (Environment and Climate Change Canada) for their production of real-time digital sea ice charts, Jean-Luc Shaw for their conversion from GIS formats, Fisheries and Oceans Canada staff at the Maurice Lamontagne Institute involved in Atlantic Zone Monitoring Program (AZMP) fall and March surveys and also those involved in maintaining the thermosalinograph system online. PSG received funding within Fisheries and Oceans Canada from the Aquatic Climate Change Adaptation Services Program (ACCASP). This work is a collaborative research contribution to Québec-Océan and the NSERC Discovery Grant program Physics of seasonal sea ice (RGPIN-2019-06563) to DD.

References

Arthun, M., Onarheim, I. H., Dörr, J., & Eldevik, T. (2021). The seasonal and regional transition to an ice-free arctic. *Geophysical Research Letters*, *48*(1), e2020GL090825. doi: https://doi.org/10.1029/2020GL090825

Black, W. A. (1958). Gulf of St. Lawrence ice survey, winter 1958. *Geographical Branch, Ottawa, Geographical Paper*, *19*, 26 pp.

Blockley, E. W., & Peterson, K. A. (2018). Improving met office seasonal predictions of arctic sea ice using assimilation of CryoSat-2 thickness. *The Cryosphere*, *12*(11), 3419–3438. doi: 10.5194/tc-12-3419-2018

Bonan, D. B., Bushuk, M., & Winton, M. (2019). A spring barrier for regional predictions of summer Arctic sea ice. *Geophysical Research Letters*, *46*(11), 5937-5947. doi: https://doi.org/10.1029/2019GL082947

Bonan, D. B., Schneider, T., Eisenman, I., & Wills, R. C. J. (2021). Constraining the date of a seasonally ice-free arctic using a simple model. *Geophysical Research Letters*, *48*(18), e2021GL094309. doi: https://doi.org/10.1029/2021GL094309

Brickman, D., & Drozdowski, A. (2012). Development and validation of a regional shelf model for Maritime Canada based on the NEM-OPA circulation model. *Canadian Technical Report of Hydrography and Ocean Sciences*, *278*, vii + 57 pp.

Brickman, D., Wang, Z., & DeTracey, B. (2016). High resolution future climate ocean model simulations for the Northwest Atlantic Shelf region. *Canadian Technical Report of Hydrography and Ocean Sciences*, *315*, 143 pp.

Canadian Ice Service. (2005). Manice: Manual of standard procedures for observing and reporting ice conditions. *ISBN 0-660-62858-9*. Retrieved from `https://publications.gc.ca/site/eng/441213/publication.html`

Cyr, F., Bourgault, D., & Galbraith, P. S. (2011). Interior versus boundary mixing of a cold intermediate layer. *J. Geophys. Res.*, *116*(C12029). doi: 10.1029/2011JC007359

Cyr, F., Snook, S., Bishop, C., Galbraith, P., Chen, N., & Han, G. (2022). Physical oceanographic conditions on the Newfoundland and Labrador Shelf during 2021. *DFO Can. Sci. Advis. Sec. Res. Doc.*, *2022/040*, iv + 48 p.

Derksen, C., Burgess, D., Duguay, C., Howell, S., Smith, L. M. S., Thackeray, C., & Kirchmeier-Young, M. (2018). Changes in snow, ice, and permafrost across

649 canada. In E. Bush & D. Lemmen (Eds.), *Canada's changing climate report*
650 (p. 194-260). Ottawa, Ontario: Government of Canada.
651 Déry, F. (1992). Interannual and intraseasanal variability of the ice cover in the Gulf
652 of Saint Lawrence, 1963-1990. *McGill University, M.Sc. Thesis*, 220 pp.
653 Deser, C., Holland, M., Reverdin, G., & Timlin, M. (2002). Decadal variations in
654 Labrador Sea ice cover and North Atlantic sea surface temperatures. *J. Geo-*
655 *phys. Res.*, *107 (C5)*, 3035. doi: 10.1029/000JC000683
656 DeTracey, B. (1993). Modelling interannual sea ice variabiiity in the Gulf of St.
657 Lawrence. *McGill University, M.Sc. Thesis*, 108 pp.
658 Galbraith, P. S. (2006). Winter water masses in the Gulf of St. Lawrence. *J. Geo-*
659 *phys. Res.*, *111*, C06022. doi: 10.1029/2005JC003159
660 Galbraith, P. S., Chassé, J., Shaw, J.-L., Dumas, J., Lefaivre, D., & Bourassa, M.-N.
661 (2023). Physical oceanographic conditions in the gulf of st. lawrence during
662 2022. *Can. Tech. Rep. Hydrogr. Ocean Sci.*, *354*, v + 88 p.
663 Galbraith, P. S., Larouche, P., & Caverhill, C. (2021). A sea-surface temperature
664 homogenization blend for the Northwest Atlantic. *Canadian Journal of Remote*
665 *Sensing*, *47:4*, 554-568. doi: 10.1080/07038992.2021.1924645
666 Galbraith, P. S., Larouche, P., Chassé, J., & Petrie, B. (2012). Sea-surface temper-
667 ature in relation to air temperature in the Gulf of St. Lawrence: interdecadal
668 variability and long term trends. *Deep-Sea Res. II*, *77-80*, 10-20.
669 Galbraith, P. S., Saucier, J., Michaud, N., Lefaivre, D., Corriveau, R., Roy, F., ...
670 Cantin, S. (2002). Shipborne monitoring of near-surface temperature and
671 salinity in the Estuary and Gulf of St. Lawrence. *Atlanctic Zone Monitoring*
672 *Program Bulletin*(2), 26-30.
673 Gilbert, D., & Pettigrew, B. (1997). Interannual variability (1948-1994) of the CIL
674 core temperature in the Gulf of St. Lawrence. *Canadian Journal of Fisheries*
675 *and Aquatic Sciences*, *54*(S1), 57–67. doi: 10.1139/cjfas-54-S1-57
676 Kanamitsu, M., Ebisuzaki, W., Woollen, J., Yang, S.-K., Hnilo, J., Fiorino, M., &
677 Potter., G. L. (2002). NCEP-DOE AMIP-II Reanalysis (r-2). *Bulletin of the*
678 *American Meteorological Society*, *Nov 2022*, 1631-1643.
679 Lavoie, D., Lambert, N., Rousseau, S., Dumas, J., Chassé, J., Long, Z., ... Azetsu-
680 Scott, K. (2020). Projections of future physical and biogeochemical conditions
681 in the Gulf of St. Lawrence, on the Scotian Shelf and in the Gulf of Maine.
682 *Canadian Technical Report of Hydrographic and Ocean Sciences*, *334*, xiii +
683 102 p.
684 Li, Y. (2000). Intraseasonal and interannual variability of sea ice in the Gulf of St.
685 Lawrence. *McGill University, Ph.D. Thesis*, 188 pp.
686 Long, Z., Perrie, W., Chassé, J., Brickman, D., Guo, L., Drozdowski, A., & Hu, H.
687 (2016). Impacts of climate change in the gulf of st. lawrence. *Atmosphere-*
688 *Ocean*, *54*(3), 337-351. doi: 10.1080/07055900.2015.1029869
689 MacIntyre, S., Romero, J. R., & King, G. W. (2002). Spatial-temporal vari-
690 ability in surface layer deepening and lateral advection in an embayment
691 of Lake Victoria, East Africa. *Limol. Oceanogr.*, *47*(3), 656-671. doi:
692 10.4319/lo.2002.47.3.0656
693 Notz, D., & SIMIP Community. (2020). Arctic sea ice in CMIP6. *Geophys-*
694 *ical Research Letters*, *47*(10), e2019GL086749. doi: https://doi.org/10.1029/
695 2019GL086749
696 Pellerin, P., Ritchie, H., Saucier, F. J., Roy, F., Desjardins, S., Valin, M., & Lee,
697 V. (2004). Impact of a two-way coupling between an atmospheric and an
698 ocean-ice model over the gulf of st. lawrence. *Monthly Weather Review*,
699 *132*(6), 1379-1398. doi: https://doi.org/10.1175/1520-0493(2004)132⟨1379:
700 IOATCB⟩2.0.CO;2
701 Peralta-Ferriz, C., & Woodgate, R. A. (2015). Seasonal and interannual vari-
702 ability of pan-Arctic surface mixed layer properties from 1979 to 2012
703 from hydrographic data, and the dominance of stratification for multiyear

mixed layer depth shoaling. *Progress in Oceanography*, *134*, 19-53. doi: https://doi.org/10.1016/j.pocean.2014.12.005

Perrie, W., Long, Z., Chassé, J., Blokhina, M., Guo, L., & Hu, H. (2015). Projected changes in surface air temperature and surface wind in the gulf of st. lawrence. *Atmosphere-Ocean*, *53*(5), 571-581. doi: 10.1080/07055900.2015.1086295

Peterson, I., Pettipas, R., & Rosing-Asvid, A. (2015). Trends and variability in sea ice and icebergs off the Canadian East coast. *Atmosphere-Ocean*, *53 (5)*, 582-594.

Peterson, I., & Prinsenberg, S. (1990). Sea ice fluctuations in the western Labrador Sea (1963-1988). *Can. Tech. Rep. Hydrogr. Ocean Sci., No. 123*. Retrieved from `https://publications.gc.ca/collections/collection_2015/mpo-dfo/Fs97-18-123-eng.pdf`

Prinsenberg, S., Peterson, I., Narayanan, S., & Umoh, J. (1997). Interaction between atmosphere, ice cover, and ocean off Labrador and Newfoundland from 1962 to 1992. *Can. J. Fish. Aquat. Sci.*, *54(Suppl. 1)*, 30-39.

Saucier, F., Roy, F., Gilbert, D., Pellerin, P., & Ritchie, H. (2003). Modeling the formation and circulation processes of water masses and sea ice in the Gulf of St. Lawrence, Canada. *J. Geophys. Res.*, *108 (C8)*, 3269. doi: 10.1029/2000JC000686

Senneville, S., & Saucier, F. J. (2007). Étude se sensibilit'e de la glace de mer au réchauffement climatique dans le Golfe et l'estuaire du Saint-Laurent. *Report to Ouranos*, 30 pp.

Shaw, J.-L., & Galbraith, P. S. (2023). Climatology of transport in the Strait of Belle Isle. *J. Geophys. Res.*, *128*(e2022JC019084). doi: 10.1029/2022JC019084

Smith, G. C., Roy, F., & Brasnett, B. (2013). Evaluation of an operational ice-ocean analysis and forecasting system for the Gulf of St Lawrence. *Quarterly Journal of the Royal Meteorological Society*, *139*(671), 419-433. doi: https://doi.org/10.1002/qj.1982

Takahashi, S., Kosugi, T., & Enomoto, H. (2011). Sea-ice extent variation along the coast of Hokkaido, Japan: Earth's lowest-latitude occurrence of sea ice and its relation to changing climate. *Annals of Glaciology*, *58(58)*. doi: 10.3189/172756411797252301

Tang, C. L., Yao, T., Perrie, W., Detracey, B., Toulany, B., Dunlap, E., & Wu, Y. (2008). BIO ice-ocean and wave forecasting models and systems for Eastern Canadian waters. *Canadian Technical Report of Hydrography and Ocean Sciences*, *261*, iv + 61 pp.

Therriault, J., Petrie, B., Pepin, P., Gagnon, J., Gregory, D., Helbig, J., ... Sameoto, D. (1998). Proposal for a northwest zonal monitoring program. *Canadian Technical Report of Hydrographic and Ocean Sciences*, *194*, vii + 57 p.

Urrego-Blanco, J., & Sheng, J. (2014). Formation and distribution of sea ice in the Gulf of St. Lawrence: A process-oriented study using a coupled ocean-ice model. *J. Geophys. Res.*, *119*, 7099-7122. doi: 10.1002/2014JC010185

Vincent, L. A., Hartwell, M. M., & Wang, X. L. (2020). A third generation of homogenized temperature for trend analysis and monitoring changes in Canada's climate. *Atmosphere-Ocean*, *58:3*, 173-191. doi: doi:10.1080/07055900.2020.1765728

WMO. (2017). WMO guidelines on the calculation of climate normals. *Tech. rep., Geneva, Switzerland*, *WMO-No. 1203*, 29 p.